Calibration of K and alpha (α) for bulk commodities

R.C.A. Minnitt[a,*], D.K. Mukhopadhyay[b], and L. Lautze[c]
[a]School of Mining Engineering, University of the Witwatersrand, Private Bag 3, WITS. 2050. Johannesburg, South Africa. Email: Richard.Minnitt@wits.ac.za
[b]Manager, Resource and Reserve Governance, South32. E-mail: Dk.Mukhopadhyay@south32.net
[c]Principal, Resource Geology, South32. E-mail: Livhuwani.Lautze@south32.net

In order to minimise the sampling error and sampling bias associated with the sampling of metal bearing ores it is essential that the heterogeneity characteristics of the ores be fully appreciated. Heterogeneity tests were carried out on the significantly different manganiferous ores produced at Wessels and Mamatwan mines near Hotazel, South Africa, for the purpose of establishing an optimal sampling protocol for the ores. The method referred to as the Segregation Free Analysis (SFA) was used for the determination of the parameters K and Alpha by construction of calibration curves. The method involves crushing a sufficient amount of ore so that after passing it through a set of fifteen nested screens there is sufficient material to then be split into 32 samples of mass 2-5 kg, using a riffle splitter, and analysing each of the samples. Thus, for fifteen nested screens there are fifteen series each consisting of 32 samples, making a total of 480 samples for analysis. Of the eighteen elements that were analysed in each sample only %Mn_3O_4, %FeO, %K_2O, %P, and %SO_2 were calibrated, the first two being the main paying elements and the last three being deleterious elements for the smelting processes in which the ores are used. Calibration curves indicate that for the coarse fraction, above 1 cm, manganese ores have alpha values close to 3, whereas those less than 1 cm in diameter have alpha values closer to 1. Reasons for this behaviour are uncertain but it could be related to the behaviour of the crystal structure in the very pure ores as the ores are progressively crushed and screened to finer size fractions. Separate nomograms were therefore prepared for the coarse and fine fractions. Net conclusions indicate that both Wessels and Mamatwan ores are relatively easy to sample and that simple two or three stage processing will suffice when preparing the final 2 g aliquot at 75 microns. Apart from minor modifications in the sample preparation protocols, there is no evidence to suggest that the Wessels and Mamatwan ores require different sample preparation protocols, or that they should be assayed differently. The calibration curves for manganese ore are compared with the calibration curves for gold bearing ores which generally have alpha values close to 1. The difference in alpha between the gold ores and bulk commodities is considered to be related to the primary distribution of the metals in nature, lognormal for gold and normal for manganese.

Introduction

Someone has said “your decisions are only as good as your samples”. The importance of this statement and effective reach is only understood once we appreciate the way in which sample data is used and applied in the mining industry, principally in the way trading in bulk commodities and base- or precious-metals is undertaken.[1,2,3,4] The principle function of a sample is to fully represent the characteristics of the lot from which it is extracted. The Theory of Sampling (TS) is a systematic multistage analytical framework, a set of unifying principles to guide the processes and stages at which samples are taken. At every stage, whether the lot is moving or stationary, TS provides principles, practices, procedures, and designs for sampling equipment, to eliminate sampling bias and minimise the sampling error (precision). TS also allows to analyse and assess the potential for individual items of sampling error and bias. The TS framework is built on evaluating common problems and features encountered in sampling different lots of different sizes in different sample settings and consists of six governing principles and four sampling unit operations that are applied in a systematic fashion to all processes, procedures, and equipment. TS is therefore a framework to guarantee accuracy and precision as well as correctness and representivity in the sample materials, from lot to aliquot.[5,6,7]

There is no inherent feature or characteristic in sample materials that allows us to classify it as representative or not – there are no red or green flags. The only way to ensure representivity is to document the history of processes and procedures used to produce the aliquot. If the process delivering the sample aliquots for analysis is correct, the sample will be representative; alternatively, if the process is incorrect, the sample can never be representative. One might ask “What are the criteria for representivity?”. This depends on the sampling method, the physical extraction process, and the extent to which the constitutional and distributional heterogeneities of the particulate matter are accounted for.[8,9,10]

In the process of selecting and recovering particulate samples the TS identifies Correct Sampling Errors (CSE), and Incorrect Sampling Errors (ISE). CSEs include the Grouping and Segregation Error (GSE) and the Fundamental Sampling Error (FSE), that contribute to total sampling error. These sampling errors arise because of the constitutional and distributional heterogeneity of the materials being sampled. Failure to understand or control sampling variances due to the particle size, shape, density, mineral composition, and target analyte content of particulate materials will result in contributions of FSE from these sources. FSE, the within fragment variability in grade, volume and density is a function of particle size (d_N), sample mass (M_S), and the nature of the material being sampled (K) according to Equation 1, which Gy[2,3,4] compiled.

$$s^2_{FSE} = \frac{K \cdot d_N}{M_S} \qquad \text{[Equation 1]}$$

According to Equation 1, the FSE can be minimised by reducing the fragment size by comminution or by increasing the sample mass. The coefficient K is the product of the mineralogical constant c, the shape factor f, the granulometry factor

doi: https://doi.org/10.1255/tosf.131

g, and the liberation factor ℓ. The principle inducements for GSE are an input of vibrational energy and gravity which act together to cause grouping and segregation of materials either by size or density, in a lot of perfectly dry materials, but the presence of moisture or sticky-ores strongly over-rides this distributional heterogeneity. The only way to reduce the Distributional Heterogeneity (GSE) is by incremental sampling and mixing. Collectively CSEs can never be eliminated, but they can be minimised by creating an optimal sampling protocol.[7,10,11]

Incorrect Sampling Errors (ISE), include Increment Delimitation Error (IDE), Increment Extraction Error (IEE), Increment Preparation Error (IPE), and the Weighting Errors (WE) which are responsible for sampling bias using poorly designed, incorrectly engineered, and badly installed sample delimitation and extraction equipment. Where particles do not have a uniform, non-zero probability of being delimited and extracted, ISEs are to be expected. Where these sampling errors and sampling biases are controlled, where an optimal sampling protocol has been applied, and a documented history of the sampling process is available, an aliquot, immediately prior to its presentation to the analytical process, is very likely to be fully representative of the lot from which it is derived, because it is the product of a correct, representative multistage sampling process.[6,7]

The aim of this paper is to present the results of heterogeneity testing of manganese ores from two mines in the Hotazel region of South Africa and to compare the sampling parameters for these bulk commodities with those for precious metals.

Review of heterogeneity tests

The first step in creating the optimal sampling protocol is the performance of a heterogeneity test which provides an understanding of the Fundamental Sampling Error (FSE). The aim of the heterogeneity test is principally to establish how the variance amongst a series of samples changes as the size of the fragments in the sample changes as the material is reduced through different stages of comminution and mass reduction on its way to the aliquot that is presented for assay. Sampling parameters K and Alpha are estimated on a size-by-size analysis of the variance of the target analyte in different size fractions of particulate materials, allowing the FSE to be calculated and controlled to acceptable levels. The heterogeneity characteristics of each material to be sampled, namely the parameters K and Alpha, are determined by compiling a calibration curve which models the way in which the variances of the target analyte change for different sized particles. Once the parameters K and alpha have been established it is then a simple task to compile the sampling nomogram which is a blue-print for the sampling protocol that defines the relationship between the variance of the Fundamental Sampling Error (FSE) and the sample mass.[12,13,14]

While there are several studies that have undertaken to determine the parameters for base and precious metals[12,14,15,16,17], the determination of sampling parameters for K and Alpha for bulk commodities, such as iron ore, manganese ores, vanadium ores, chromite ores are not widely publicised. The reasons for the lack of reported heterogeneity tests for bulk commodities is probably due to the relatively forgiving sampling characteristics of these ores compared to the complexities associated with precious and base metal ores. The target analyte, Fe or Mn, in bulk materials for example is contained in the minerals haematite or braunite-pyrolusite-bixbyite constituting the ore, and there is no effective liberation factor. Where the target analyte is contained as minute grains of mineral or metal, distinct and separate from the host, the liberation factor is an extremely important contributor to the constitutional heterogeneity.

There is a wide spectrum of different approaches for performing Heterogeneity Tests.[4,5,6,7,8] For this particular exercise the so-called Segregation Free Analysis (SFA) method described in detail by Minnitt[12,13,14,15] is used. The SFA method is a simple extension of the Duplicate Series Analysis (DSA) method proposed by Bongarçon[15,16,17], the main difference being that the SFA method separates the crushed materials for the heterogeneity test into different size classes.

Heterogeneity tests for bulk commodities

As part of a review of the sampling facilities and procedures at the Wessels and Mamatwan mines near Hotazel, South Africa, it was suggested that Heterogeneity Tests be carried out on the manganiferous ores produced at the mines. The manganese bearing ores produced at the mines are sufficiently different to warrant that the Heterogeneity Tests be carried out on both ore types. Of the several methods for performing Heterogeneity Tests, the Segregation Free Analysis (SFA) method was used for determining the parameters K and Alpha by construction of calibration curves for the differing ore types produced at Wessels and Mamatwan mines. Approximately 180 kg of high-grade, run-of-mine manganese ore from the Wessels and Mamatwan mines was crushed and screened through 15 individual screens ranging in size from 37.5 mm to 0.05 mm; it is essential that the largest fragment sizes are accurately represented in the heterogeneity test.

Finer materials were passed through the nested screens (Figure 1a) using a mechanical shaker (Figure 1b), and the fragments on top of each screen were selected for a given size fraction. After crushing the ore to appropriate sizes, the material was screened through 15 screens for Wessels ores and 14 screens for Mamatwan ores. The material retained on top of each screen size was then passed through a riffle splitter to give 32 samples for each size fraction.

(a) (b)

Figure 1: (a) Nested screens for separating ores into correct size fractions, and (b) the mechanical sieve shaker

The distribution of the mass for each of the screened size fractions is shown in Figures 2a and 2b for the Wessels and Mamatwan mines, respectively.

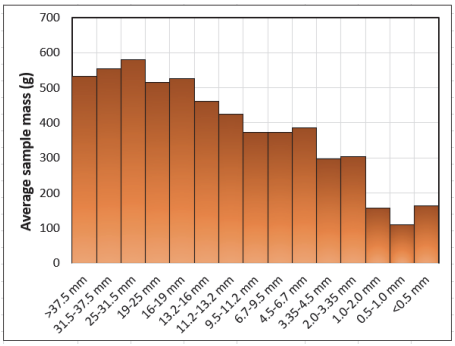

2 (a) Wessels ores

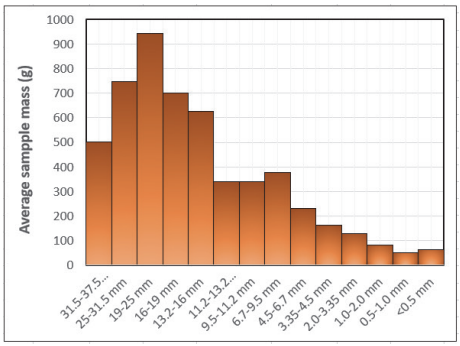

2 (b) Mamatwan ores

Figure 2: (a) Average sample mass for each of 15 size fractions of Wessels ores, and (b) average sample mass for each of 14 size fractions of Mamatwan ores

Ideally one would want the distribution of the mass of fragment sizes to be somewhat flatter than shown in Figures 2a and 2b, as there is too much material in the higher size fractions and to little material in the lower size fractions to get an acceptable sample mass when the size fractions are split into the 32 sample fractions. In order to achieve this some of the excess material in the larger size fractions was crushed and again passed through the screens to distribute the material to smaller size fractions.

Once the Mamatwan and Wessels ores had been divided into 14 and 15 series of samples, respectively, each of the series was then split into 32 individual samples. The series containing larger fragment sizes had fewer fragments per sample, whereas the smaller fragment sizes contained numerous fragments. Each sample was intended for an experimental point in the calibration curves used to determine the values of K and Alpha (α) for use in Gy's Formula for determination of the Fundamental Sampling Error and construction of the sampling nomogram for the Wessels and Mamatwan ore-types.

Sample preparation protocol for Wessels and Mamatwan ores

The sample preparation protocol for the heterogeneity test for the Wessels and Mamatwan ores was identical. For the larger fragments, the preparation protocol is shown in a series of photographs in Figure 2. The main assumption of the Heterogeneity Test is that there should be no auto-correlation between samples collected to perform the test. Fragments making up each sample are individually selected at random to remove any distributional heterogeneity and minimise the contribution from the grouping and segregation error. In order to achieve this, large fragments (>31.5 mm) were laid out on a table one fragment deep (Figure 3a) so that each and any fragment was accessible for selection. The fragments were collected at random as 4 people (Figure 3b) moved around the table and collected a specified number of fragments to produce an appropriate sample mass (Figure 3c and 3d).

(a) (b)

(c) (d)

Figure 3: (a) Coarse ore fragments laid on table, (b) the sampling team in preparation for selecting coarse ore fragments at random, (c) as the team moves around the table, they select a given number of fragments at random to achieve the correct sample mass, and (d) the team moves around the table collecting fragments at random

Finer grained manganese ores were split into the 32 samples using riffle splitters with vane widths in keeping with the sizes of the material fragments being sampled, an 8-vane splitter for fractions greater than 10 mm (Figure 4a) and a 20-vane splitter for fractions less than 10 mm (Figure 4b).

(a) (b)

Figure 4: (a) Riffle splitter for coarse materials, >10 mm, and (b) riffle splitter for fine materials, <10 mm

Following the splitting process, the samples are bagged (Figure 5a), weighed (Figure 5b), and prepared for dispatch to the analytical laboratories (Figure 5c).

(a) (b) (c)

Figure 5: (a) Bagged samples, (b) all samples are weighed, and (c) Samples are packed ready for transport to the laboratory for analysis

An example of the closely screened manganese ore materials between 2.00 mm and 3.35 mm is shown in Figure 6.

Figure 6: Closely screened manganese ore materials between 2.00 mm and 3.35 mm, with an average d_N = 2.659 mm

The average nominal top-size of a fraction retained between screens of 1.266 cm and 0.63 cm is calculated as follows:

Top screen (cm	Bottom screen (cm)
1.266	0.63

$$d_N = \sqrt[3]{\frac{d^3_{upper\ screen\ size} + d^3_{lower\ screen\ size}}{2}} \qquad \text{[Equation 2]}$$

$$= \sqrt[3]{\frac{1.266^3 + 0.63^3}{2}} = \sqrt[3]{1.1396} = 1.0445\ cm$$

Using Equation 2, the average nominal top-size for the material shown in Figure 6 is calculated as 2.659 mm.

Heterogeneity test for manganese ores

An estimate of the sampling parameters *K* and alpha (α) for an ore type allows one to calculate the FSE and provide an indication of the minimum sample mass for a given fragment size according to Equation 1. With these sampling parameters it is then possible to calculate the sampling nomogram for these specific ores. Equation [1] is rearranged in the following manner to give Equation [3] which represents a straight-line equation relating the standardised variance and the top size of the fragments in the fifteen series of data analysed.[16,17,18]

$$\ln(\sigma_R^2 \times M_S) = \alpha \ln d_N + \ln(K) \qquad \text{[Equation 3]}$$

By calculating the standardised variance and the top-size of fragments in $\log_e$ terms each set of fifteen analyses should plot along a straight line of the form $y = mx + c$.

Analytical results for each of the 32 samples in each of the series submitted for analysis were received for the elements $\%Mn_3O_4$, %FeO, $\%K_2O$, %P, and $\%SO_2$. The $\%Mn_3O_4$ results for 32 samples across all fragments sizes are shown in Appendix 1. The total mass of sample materials received at the Mamatwan and Wessels assay laboratories for fusion and pressed pellet analysis are listed in Table 1.

Table 1: Total mass received at Wessels and Mamatwan assay laboratories for fusion and pressed pellet analysis

Laboratory	Total mass of sample received	Mass for fusion analysis	Mass for pressed pellet analysis
Wessels	100g	2g	30g
Mamatwan	200g	2g	30g

Modeling process

The modeling process is a stepwise inspection of the lists of analytical data used in the calculation of the variances to be used in the calibration process. An example of statistics calculated for $\%Mn_3O_4$ from Series 2 (W2), for a fragment size of 3.4755 cm (Appendix 1), is shown in Table 2, while an example of the calculations and description of items named in the calculation table, is presented in Table 3. The modeling process requires that each assay value be considered individually and that the effects of removing suspicious values on the calibration curve should be examined. The modeling process is not simply a matter of populating a template with the sample calculations, but rather a matter of examining each set of data and examining whether or not a specific value belongs in the data set and how its inclusion or removal will affect the calibration curve. This process was carried out for each list of assay data for each of the calibration curves. In some cases, the decision to exclude certain data is always somewhat controversial. It should however be remembered that the process aims to establish a viable and acceptable model based on the data.

Table 2: Example of statistics calculated for $\%Mn_3O_4$ from Series 2 (W2), for fragment size 3.4755 cm,

Statistics for for $\%Mn_3O_4$	W2
Mean	65.5161
Variance	38.0878
Std Dev	6.1715
Relative standard deviation	0.0942
Top screen (cm)	3.4755
Bottom screen (cm)	2.8616
Size (cm)	3.4755
Average Mass (g)	566.5000

The basic statistics shown in Table 1 are then analysed and prepared for plotting on the calibration curve according to the routine shown in Table 2.

Table 3: Example of calculations and description of items named in the calculation table for $\%Mn_3O_4$, example from Series 2 (W2), for fragment size 3.4755 cm (Appendix 1)

Item	Value	Explanation
d_{p95} (cm)	3.47546	Fragment top-size is a value determined for the largest 5% of fragments in a sample
Measured Multi-stage rsd	0.09420	The relative standard deviation (rsd = Std dev/mean) for the multiple stages of handling that a sample has been subject to, prior to fire assay.
Measured Multi-stage Var	0.00887	The square of the Measured Multistage relative standard deviation, to give the Measured Multistage variance.
Less Analytical Var	0.00887	This is a standard variance calculated from the precision usually quoted by an analytical laboratory; the generally inflated value from commercial laboratories is in the order of 9%.
Standardised Var	0.58130	The Measured Multistage variance less the Analytical variance is multiplied by the mean to return the value to a standardised multistage variance, rather than a relative variance.
Mass (g)	566.50000	This is the mass of the sample, prior to preparation steps involving crushing and splitting in the assay laboratory.
s^2*M_s	329.30438	This is the Fundamental sampling variance multiplied by the sample mass.
$\ln(s^2*M_s)$	5.79698	This is the LN value for the Fundamental sampling variance multiplied by the sample mass
$\ln(d_{max})$	1.24573	This is the LN value for the fragment size
Note that the last two values are plotted on the abscissa (x-axis) and ordinate (y-axis) of the calibration curve		

Analysis of the calibration experiments carried out for the elements for $\%Mn_3O_4$, %FeO, $\%Al_2O_3$, %CaO, $\%K_2O$, %P, and $\%SO_2$ was undertaken with the values for $\ln(s^2*M_s)$ and $\ln(d_{max})$ for each element being listed in Table 4. Calibration curves for each of these elements were compiled from the analytical results for each of these elements in Figures 7 to 11.

Table 4: Compilation of values for $\ln(s^2*M_s)$ and $\ln(d_{max})$ for each element $\%Mn_3O_4$, %FeO, $\%K_2O$, %P and $\%SO_2$ for Mamatwan (top row) and Wessels (bottom row) mines

Mamatwan	$\%Mn_3O_4$	
Size fraction	$\ln(d_{max})$	$\ln(s^2*M_s)$
1	1.39	4.62
2	1.25	4.31
3	1.05	3.69
4	0.81	2.88
5	0.57	2.54
6	0.39	2.11
7	0.21	0.97
8	0.04	0.72
9	-0.18	0.01
10	-0.53	-0.62
11	-0.88	-1.49
12	-1.26	-3.02
13	-1.80	-3.07
14	-2.49	-2.91

Mamatwan	%FeO	
Size fraction	$\ln(d_{max})$	$\ln(s^2*M_s)$
1	1.39	3.68
2	1.25	3.44
3	1.05	2.88
4	0.81	2.04
5	0.57	1.42
6	0.39	1.59
7	0.21	1.42
8	0.04	0.44
9	-0.18	-0.96
10	-0.53	-1.54
11	-0.88	-2.63
12	-1.26	-4.11
13	-1.80	-4.78
14	-2.49	-4.33

Mamatwan	$\%K_2O$	
Size fraction	$\ln(d_{max})$	$\ln(s^2*M_s)$
1	1.39	0.58
2	1.25	-1.53
3	1.05	0.54
4	0.81	-1.98
5	0.57	-1.52
6	0.39	-3.49
7	0.21	-0.59
8	0.04	-1.02
9	-0.18	-4.52
10	-0.53	-4.39
11	-0.88	-4.73
12	-1.26	-1.64
13	-1.80	-2.35
14	-2.49	-1.75

Mamatwan	%P	
Size fraction	$\ln(d_{max})$	$\ln(s^2*M_s)$
1	1.39	-3.10
2	1.25	-2.40
3	1.05	-2.44
4	0.81	-3.07
5	0.57	-3.48
6	0.39	-4.32
7	0.21	-3.98
8	0.04	-4.12
9	-0.18	-4.77
10	-0.53	-5.66
11	-0.88	-5.30
12	-1.26	-6.45
13	-1.80	-6.10
14	-2.49	-5.58

Mamatwan	$\%SO_4$	
Size fraction	$\ln(d_{max})$	$\ln(s^2*M_s)$
1	1.39	2.03
2	1.25	1.38
3	1.05	2.97
4	0.81	1.56
5	0.57	1.78
6	0.39	1.01
7	0.21	1.17
8	0.04	-0.41
9	-0.18	-0.87
10	-0.53	-1.57
11	-0.88	-1.51
12	-1.26	-2.63
13	-1.80	-2.05
14	-2.49	-2.60

Wessels	$\%Mn_3O_4$	
Size fraction	$\ln(d_{max})$	$\ln(s^2*M_s)$
1	1.39	6.45
2	1.25	5.80
3	1.05	4.95
4	0.81	4.37
5	0.57	3.65
6	0.39	3.16
7	0.21	2.29
8	0.04	2.29
9	-0.18	1.99
10	-0.54	0.49
11	-0.91	0.04
12	-1.26	-0.67
13	-1.80	-1.48
14	-2.49	-2.31
15	-3.00	-2.22

Wessels	%FeO	
Size fraction	$\ln(d_{max})$	$\ln(s^2*M_s)$
1	1.39	6.98
2	1.25	5.86
3	1.05	5.68
4	0.81	4.91
5	0.57	4.66
6	0.39	3.77
7	0.21	3.38
8	0.04	3.04
9	-0.18	2.38
10	-0.54	0.84
11	-0.91	0.81
12	-1.26	-0.09
13	-1.80	-1.10
14	-2.49	-1.41
15	-3.00	-0.04

Wessels	$\%K_2O$	
Size fraction	$\ln(d_{max})$	$\ln(s^2*M_s)$
1	1.39	5.87
2	1.25	4.59
3	1.05	3.35
4	0.81	3.77
5	0.57	3.03
6	0.39	1.66
7	0.21	1.33
8	0.04	0.44
9	-0.18	0.66
10	-0.54	-0.19
11	-0.91	0.76
12	-1.26	1.10
13	-1.80	0.32
14	-2.49	-2.13
15	-3.00	-1.41

Wessels	%P	
Size fraction	$\ln(d_{max})$	$\ln(s^2*M_s)$
1	1.39	0.87
2	1.25	1.34
3	1.05	-0.25
4	0.81	-0.70
5	0.57	-0.66
6	0.39	-1.88
7	0.21	-2.49
8	0.04	-2.24
9	-0.18	-3.11
10	-0.54	-3.34
11	-0.91	-3.71
12	-1.26	-4.01
13	-1.80	-5.01
14	-2.49	-4.90
15	-3.00	-4.56

Wessels	$\%SO_4$	
Size fraction	$\ln(d_{max})$	$\ln(s^2*M_s)$
1	1.39	6.04
2	1.25	5.27
3	1.05	5.07
4	0.81	4.38
5	0.57	3.46
6	0.39	2.16
7	0.21	2.28
8	0.04	1.88
9	-0.18	0.69
10	-0.54	0.66
11	-0.91	0.93
12	-1.26	0.13
13	-1.80	-0.98
14	-2.49	-1.99
15	-3.00	-0.58

Compilation of the calibration curves

Calibration curves for the elements $\%Mn_3O_4$, $\%FeO$, $\%K_2O$, $\%P$, and $\%SO_2$ for Mamatwan and Wessels as listed in Table 4, are shown in Figures 7 to 11; calibration curves for Mamatwan ores are shown in red, while those for the Wessels data are shown in yellow. In view of the obvious inflection in the calibration curves at an approximate fragment size of 0.9 cm, the curves have been split into calibration points with fragments greater than 0.9 cm, and those whose fragment size is less than 0.9 cm. As a result, for each element shown in Figures 7 to 11, three modelling curves are shown, (a) a model using all the data (upper panel), (b) a model using only fragments larger than 0.9 cm, and (c) a model using only fragments less than 0.9 cm. The calibration curves modelled in the upper panels of each figure used all the available data. The data was split at the inflection points in the curve, above and below the point where the fragment size is about 0.9 cm. Models for fragment sizes >0.9 cm shown in the lower LHS panel (b), generally have steeper slopes, while models for fragment sizes <0.9 cm shown in the lower RHS panels (c), have much flatter slopes. The straight-line equations for the Wessels data are shown in the upper LHS of the calibration curves, while those for the Mamatwan data are shown in the lower RHS of the calibration curves in Figures 7 to 11.

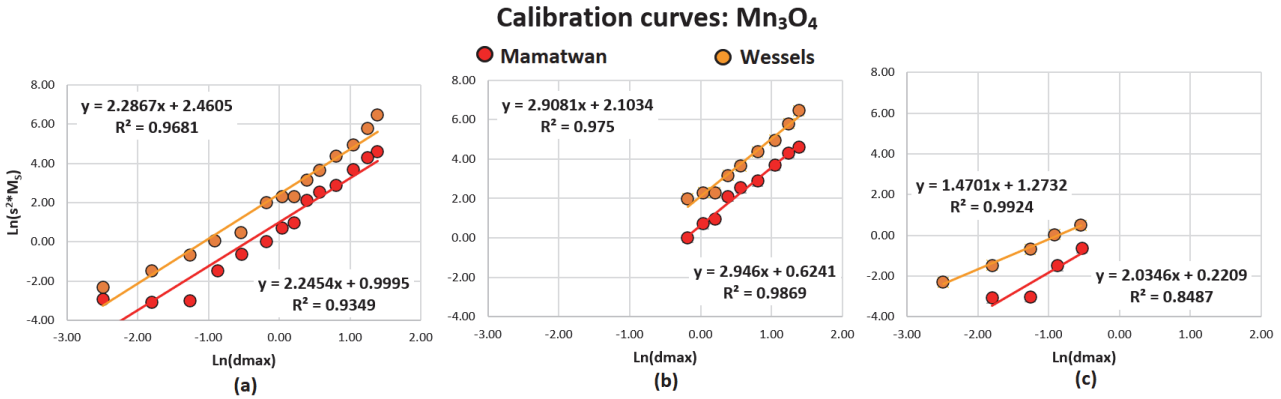

Figure 7: Calibration curves for $\%Mn_3O_4$ for Wessels (orange points) and Mamatwan (red points) ore-types: (a) unadjusted model in upper panel, (b) adjusted models for fragments >0.9 cm in lower LHS panel, and (c) adjusted models for fragments <0.9 cm in lower RHS panel. Linear trendlines-upper LHS for Wessels ores, lower RHS for Mamatwan ores

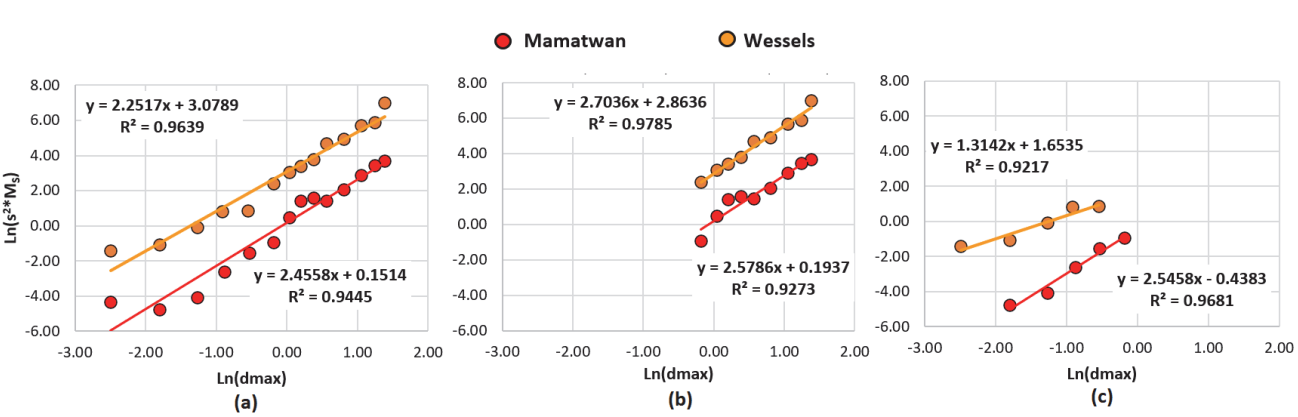

Figure 8: Calibration curves for %FeO for Wessels (orange points) and Mamatwan (red points) ore-types: (a) unadjusted model in upper panel, (b) adjusted models for fragments >0.9 cm in lower LHS panel, and (c) adjusted models for fragments <0.9 cm in lower RHS panel. Linear trendlines-upper LHS for Wessels ores, lower RHS for Mamatwan ores

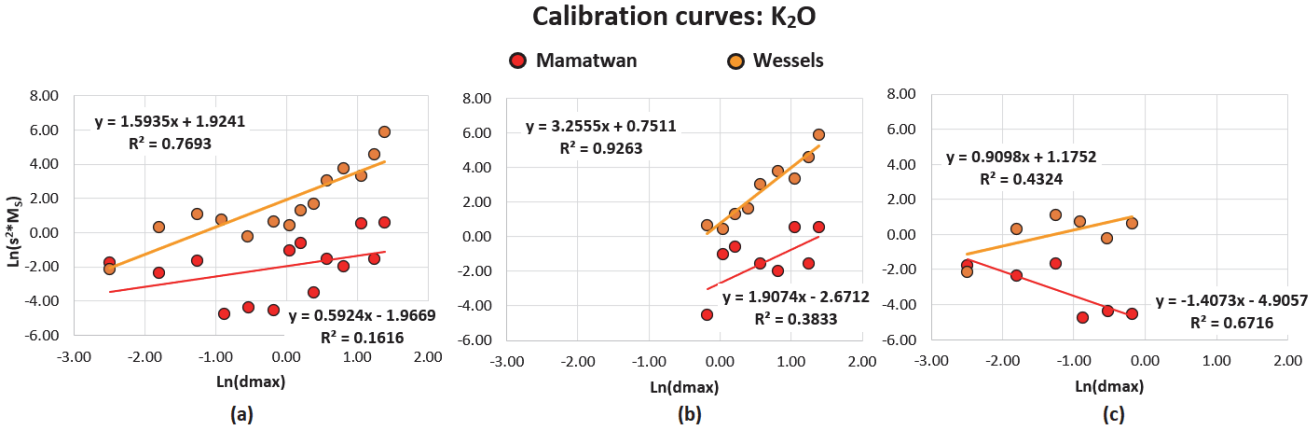

Figure 9: Calibration curves for %K_2O for Wessels (orange points) and Mamatwan (red points) ore-types: (a) unadjusted model in upper panel, (b) adjusted models for fragments >0.9 cm in lower LHS panel, and (c) adjusted models for fragments <0.9 cm in lower RHS panel. Linear trendlines-upper LHS for Wessels ores, lower RHS for Mamatwan ores

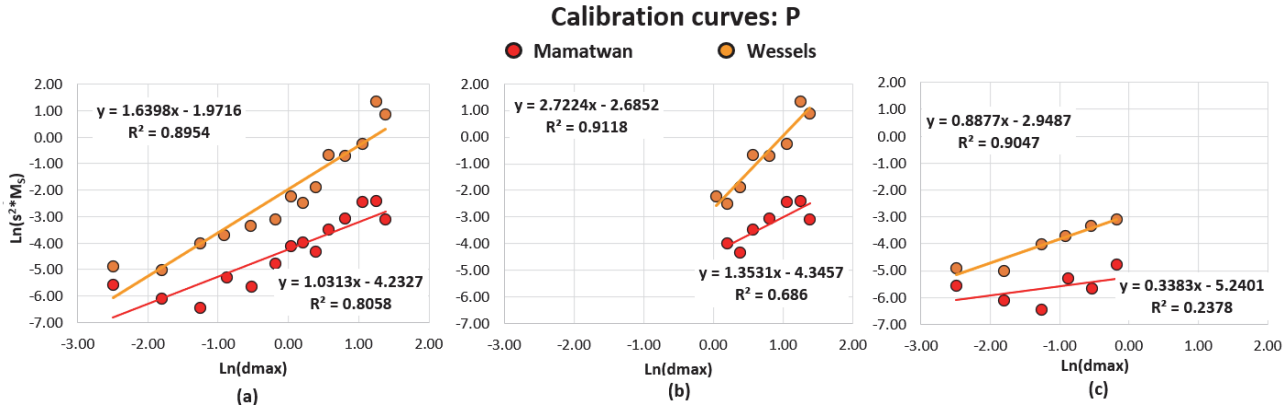

Figure 10: Calibration curves for %P for Wessels (orange points) and Mamatwan (red points) ore-types: (a) unadjusted model in upper panel, (b) adjusted models for fragments >0.9 cm in lower LHS panel, and (c) adjusted models for fragments <0.9 cm in lower RHS panel. Linear trendlines-upper LHS for Wessels ores, lower RHS for Mamatwan ores

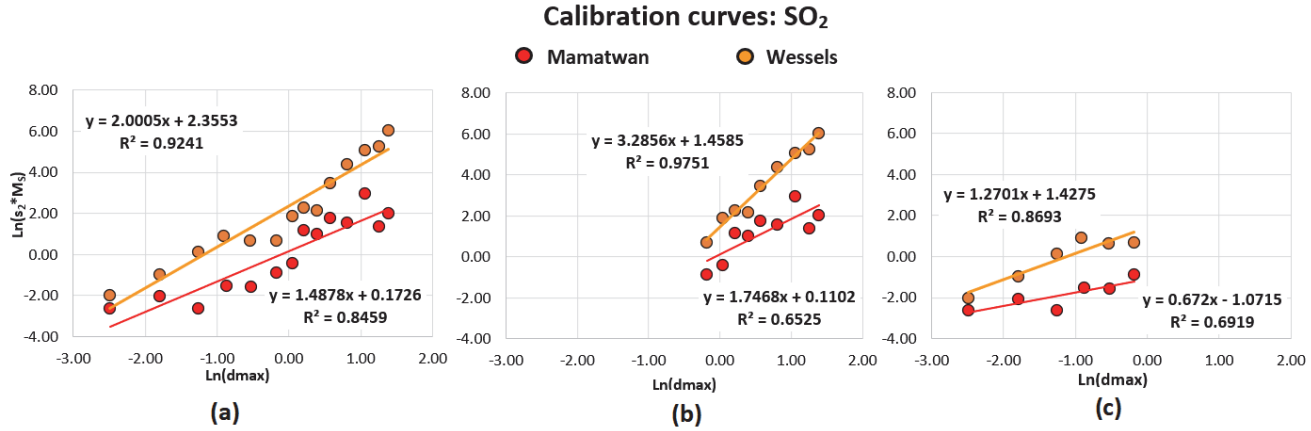

Figure 11: Calibration curves for %SO_2 for Wessels (orange points) and Mamatwan (red points) ore-types: (a) unadjusted model in upper panel, (b) adjusted models for fragments >0.9 cm in lower LHS panel, and (c) adjusted models for fragments <0.9 cm in lower RHS panel. Linear trendlines-upper LHS for Wessels ores, lower RHS for Mamatwan ores

Values for the slope Alpha (α), intercept K, and the R^2 values taken from trendlines through the calibration points are summarised in Table 5. For each of the elements analysed the R^2 value is considerably improved for all the curves showing only the coarser fragment sizes. Another feature is that Alpha (α), the average slope for all elements, in the coarser grained materials for Mamatwan and Wessels, increases from 1.57 to 2.11 and from 1.95 to 2.98, respectively. In a similar way the average slope for all elements in the finer grained materials for Mamatwan and Wessels, decreases from 1.57 to 0.84 and from 1.95 to 1.17, respectively. This indicates that the rate of change in variance is more marked for coarser materials than for the finer.

It is also notable that the average intercept (K) for all elements (except %P) in the coarser grained materials for Mamatwan and Wessels, decreases from 1.30 to 1.07 and from 12.71 to 8.03, respectively. In a similar way the average intercept (K) for all elements in the finer grained materials for Mamatwan and Wessels, decreases from 1.30 to 0.29 and from 12.71 to 4.05, respectively. Decreases in the average intercept (K) means that there is less likelihood that the sample nomogram will breach the 10% Safety Line.

Table 5: Summary of calibration parameters for the slope Alpha (α), the intercept on the Y-axis K, and the R^2 for all available data, for fragment sizes >0.9 cm and <0.9 cm derived from the calibration curves shown in Figures 7 to 11 for the elements %Mn_3O_4, %FeO, %K_2O, %P, and %SO_2 from the Mamatwan and Wessels mines

	Using all data		Fragment sizes >0.9 cm		Fragment sizes <0.9 cm	
$\%Mn_3O_4$	Mamatwan	Wessels	Mamatwan	Wessels	Mamatwan	Wessels
Alpha	2.2867	2.2454	2.946	2.9081	2.0346	1.4701
lnK	0.9995	2.4605	0.6241	2.1034	0.2209	1.2732
K	2.7169	11.7107	1.8666	8.1940	1.2472	3.5723
R2	0.9349	0.9681	0.9869	0.9349	0.8487	0.9924

	Using all data		Fragment sizes >0.9 cm		Fragment sizes <0.9 cm	
%FeO	Mamatwan	Wessels	Mamatwan	Wessels	Mamatwan	Wessels
Alpha	2.4558	2.2517	2.5786	2.7036	2.5458	1.3142
lnK	0.1514	3.0789	0.1937	2.8636	-1.0791	1.6535
K	1.1635	21.7345	1.2137	17.5245	-0.4383	5.2252
R2	0.9445	0.9639	0.9273	0.9785	0.9681	0.9217

	Using all data		Fragment sizes >0.9 cm		Fragment sizes <0.9 cm	
$\%K_2O$	Mamatwan	Wessels	Mamatwan	Wessels	Mamatwan	Wessels
Alpha	0.5924	1.5935	1.9074	3.2555	-1.4073	0.9098
lnK	-1.9669	1.9241	-2.6712	0.7511	-4.9057	1.1752
K	0.1399	6.8490	0.0692	2.1193	0.0074	3.2388
R2	0.1616	0.7693	0.3833	0.9263	0.6716	0.4324

	Using all data		Fragment sizes >0.9 cm		Fragment sizes <0.9 cm	
%P	Mamatwan	Wessels	Mamatwan	Wessels	Mamatwan	Wessels
Alpha	1.0313	1.6398	1.3531	2.7224	0.3383	0.8877
lnK	-4.2327	-1.9716	-4.3457	-2.6852	-5.2401	-2.9487
K	0.0145	0.1392	0.0130	0.0682	0.0053	0.0524
R2	0.8058	0.8954	0.686	0.9118	0.2378	0.9047

	Using all data		Fragment sizes >0.9 cm		Fragment sizes <0.9 cm	
$\%SO_2$	Mamatwan	Wessels	Mamatwan	Wessels	Mamatwan	Wessels
Alpha	1.4878	2.005	1.7468	3.2856	0.672	1.2701
lnK	0.1726	2.3553	0.1102	1.4585	-1.0715	1.4275
K	1.1884	10.5413	1.1165	4.2995	0.3425	4.1683
R2	0.8459	0.9241	0.6525	0.9751	0.6919	0.8693

Calibration curves indicate that for $\%Mn_3O_4$ and for %FeO the coarse fraction, above 0.9 cm, manganese ores have alpha values close to 3, whereas those less than 0.9 cm in diameter have alpha values closer to 1. Indications from the calibration curves shown in Figures 7 to 11 for elements under consideration are that Alpha (α) and K values are substantially changed indicating that the sampling nomogram for coarser grained materials (>0.9 cm) will be different from that for finer grained materials (<0.9 cm). Generally, the Wessels ores with an average *K* coefficient of 12.71, is about 9 times larger than that for Mamatwan ores (1.30), which will also significantly affect nomograms for the two ore types. A visual inspection of the calibration curves indicates a considerable improvement in the R^2 value for all the curves once the adjustments have been made to the data in the very smallest grain sizes, usually the 0.17 cm and 0.08 cm fractions.

Compilation of the sampling nomograms

The values for K and Alpha derived from the modelled calibration curves for the elements $\%Mn_3O_4$, %FeO, $\%K_2O$, %P, and $\%SO_2$ are listed in Table 5. The intercept on the Y-axis in the calibration curves is transformed into the Intercept K using the exponent function; all calculations are carried out to four decimal places and rounded down to two. These data are used to compile the nomograms for cross-stream sampling of the ores, for the different elements considered for the Wessels and Mamatwan ores. Sampling nomograms for Mamatwan (upper panel) and Wessels (lower panel) ores for the elements $\%Mn_3O_4$, %FeO, $\%K_2O$, %P, and $\%SO_2$ are shown in Figures 12 to 16, (a and d) using all available data, (b and e) for coarse grained fragments > 0.90 cm, and (c and f) for fine-grained fragments < 0.90 cm. An example of the nomogram calculation using K, Alpha (α), lot mass, and fragments size, values which are substituted into Equation 1, is shown for the sample preparation nomogram and the improved nomogram in Table 6.

Table 6: An example of the sample nomogram and improved nomogram calculation for $\%Mn_3O_4$ in Mamatwan ores

Mamatwan	$\%Mn_3O_4$	
Slope, Alpha=	2.24	
Intercept, K=	0.93	2.54

Sample Preparation Nomogram: $\%Mn_3O_4$		
Mass (g)	Fragment size (cm)	Precision
24000.0	7.00	0.00827
24000.0	1.0000	0.00011
500.0	1.0000	0.00508
500.0	0.0075	0.00000
2.0	0.0075	0.00002

Improved Sample Nomogram: $\%Mn_3O_4$		
Mass (g)	Fragment size (cm)	Precision
24000.0	2.00	0.00050
24000.0	0.5000	0.00002
500.0	0.5000	0.00108
500.0	0.0500	0.00001
2.0	0.0500	0.00155

Of the eighteen elements that were analysed in each sample calibration curves were only compiled for the elements %Mn_3O_4, %FeO, %K_2O, %P, and %SO_2, the first two being the main elements and the last three being the deleterious elements. These elements probably have reasonably stringent specification limits from an operational view point..

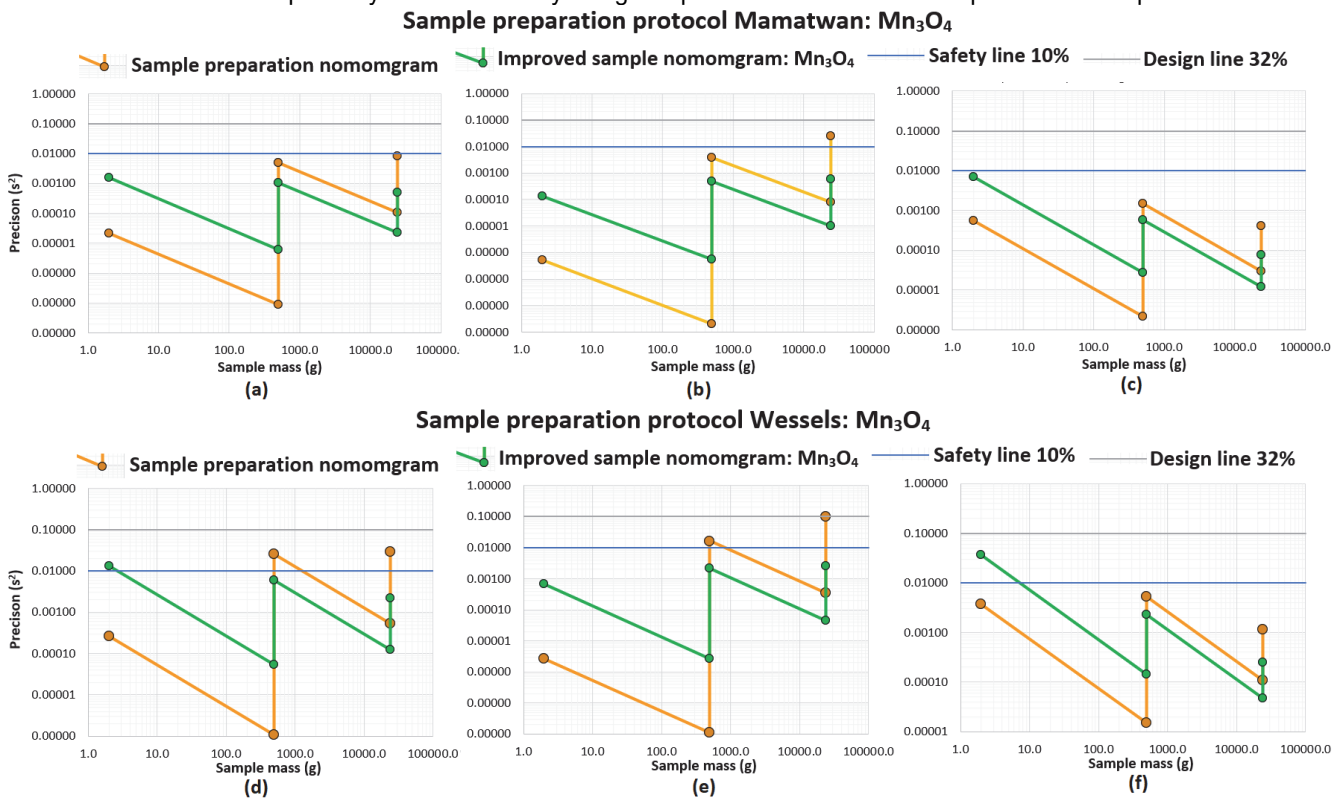

Figure 12: Sampling nomograms for Mamatwan (upper panel) and Wessels (lower panel) ores for the element %Mn_3O_4 (a and d) using all available data, (b and e) for coarse grained fragments > 0.90 cm, and (c and f) for fine-grained fragments < 0.90 cm

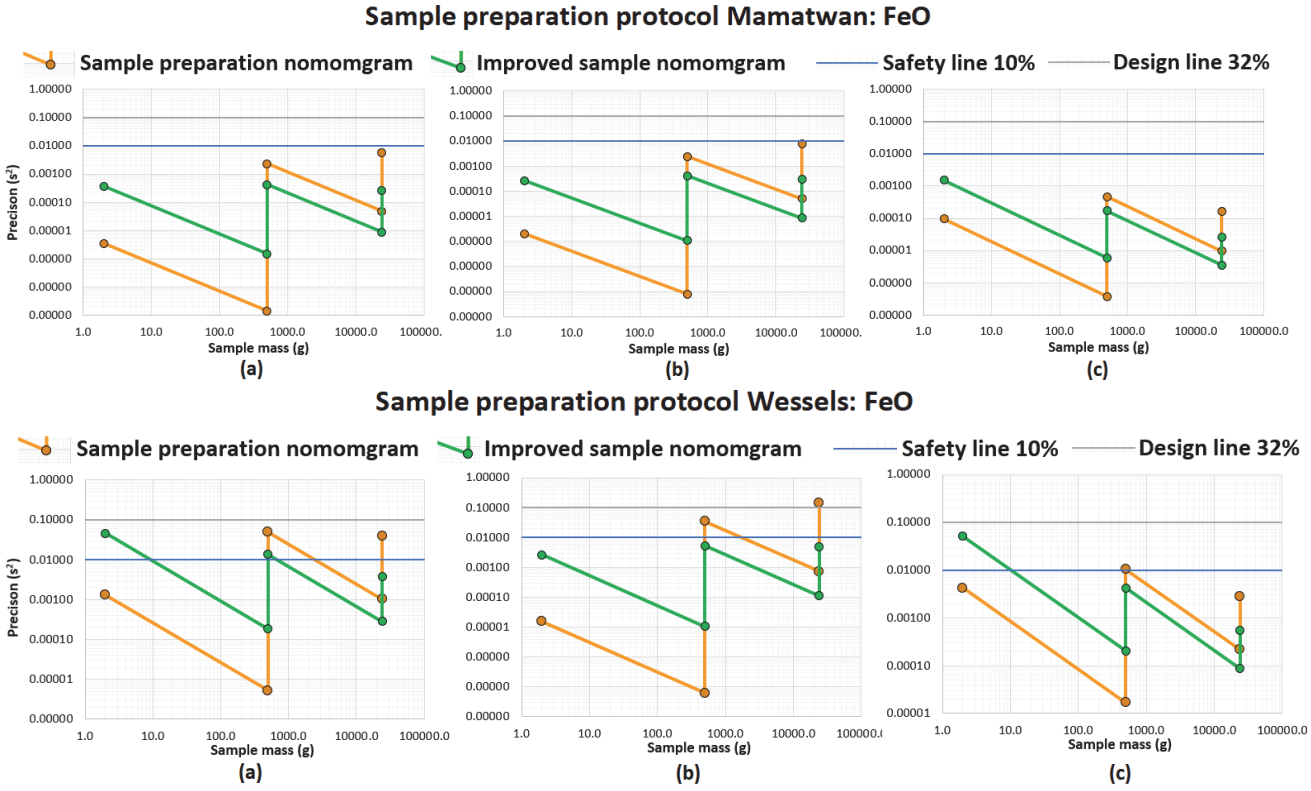

Figure 13: Sampling nomograms for Mamatwan (upper panel) and Wessels (lower panel) ores for the element %FeO (a and d) using all available data, (b and e) for coarse grained fragments > 0.90 cm, and (c and f) for fine-grained fragments < 0.90 cm

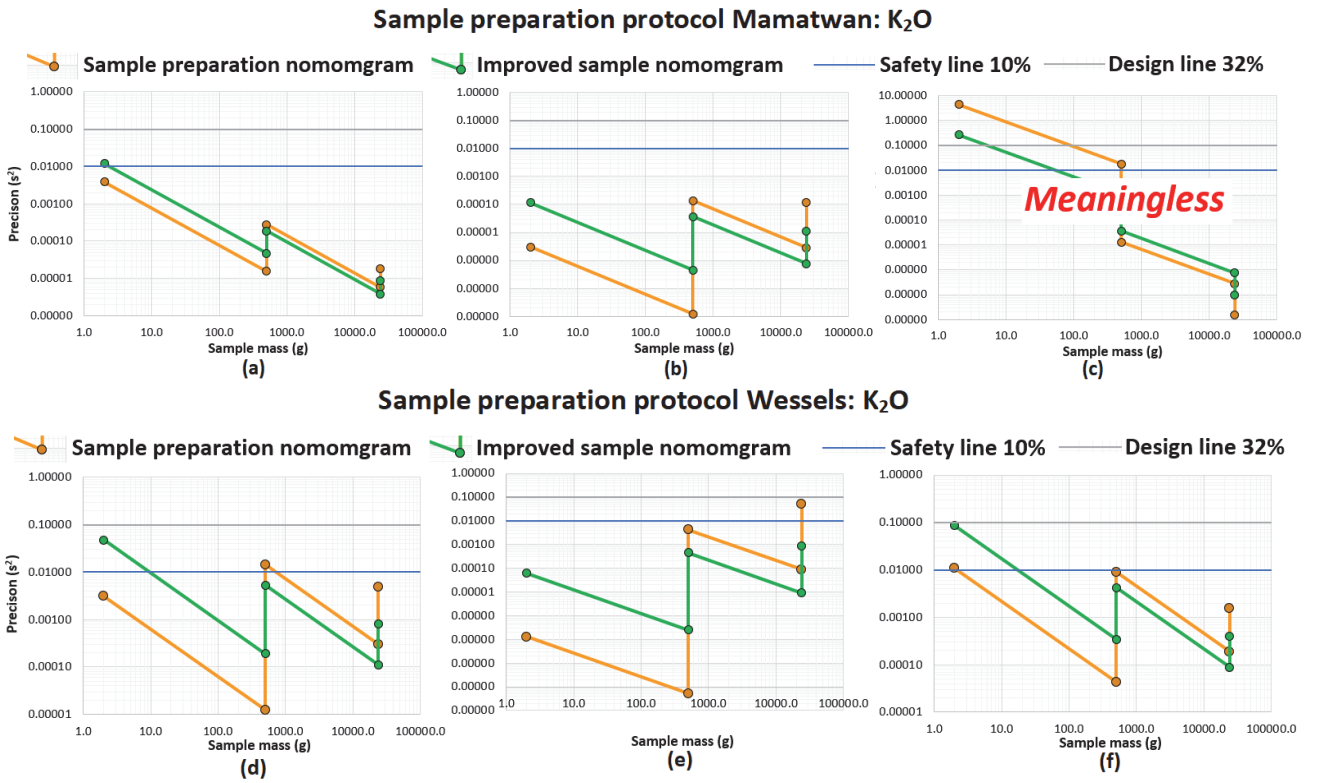

Figure 14: Sampling nomograms for Mamatwan (upper panel) and Wessels (lower panel) ores for the element %K_2O (a and d) using all available data, (b and e) for coarse grained fragments > 0.90 cm, and (c and f) for fine-grained fragments < 0.90 cm

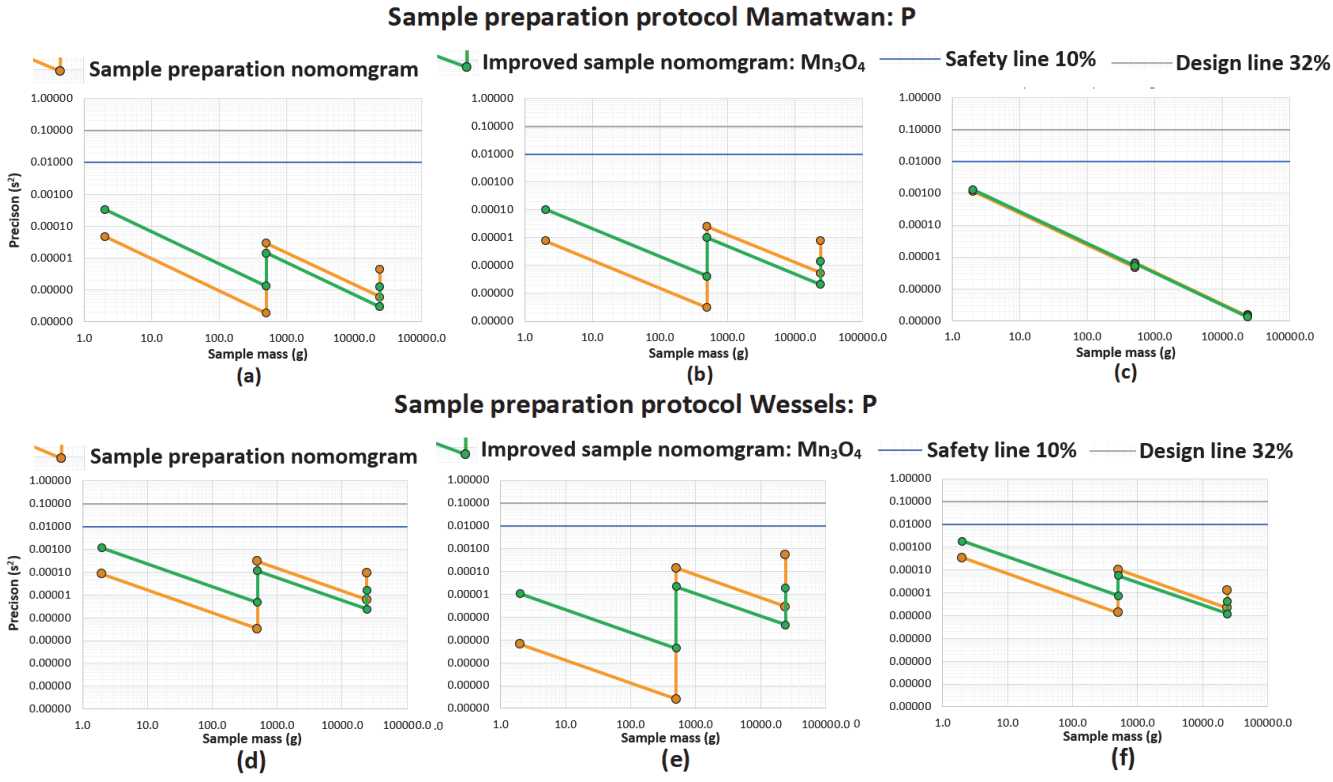

Figure 15: Sampling nomograms for Mamatwan (upper panel) and Wessels (lower panel) ores for the element %P (a and d) using all available data, (b and e) for coarse grained fragments > 0.90 cm, and (c and f) for fine-grained fragments

< 0.90 cm

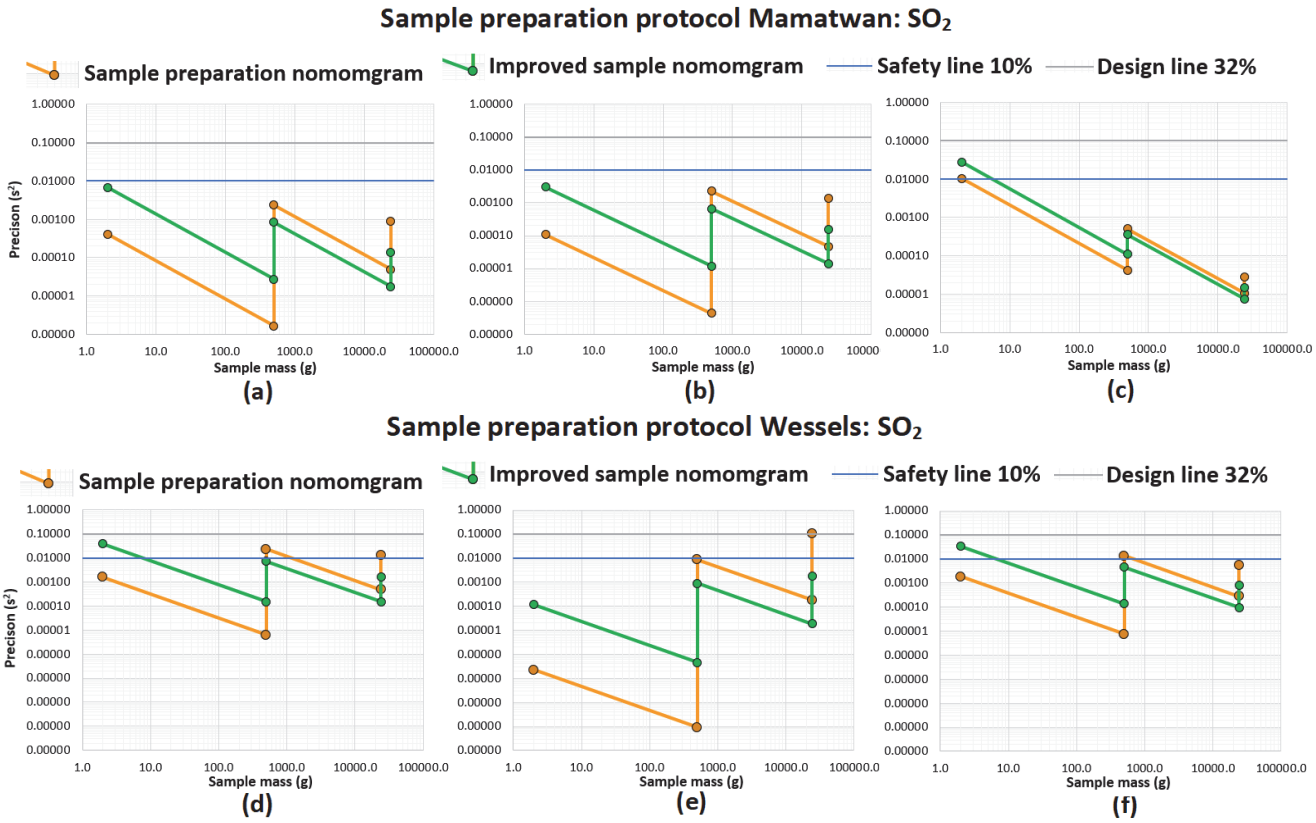

Figure 16: Sampling nomograms for Mamatwan (upper panel) and Wessels (lower panel) ores for the element %SO_2 (a and d) using all available data, (b and e) for coarse grained fragments > 0.90 cm, and (c and f) for fine-grained fragments < 0.90 cm

The sampling nomograms provide definitive steps for ensuring that the preparation of the sample, from lot to aliquot takes place in a way that does not violate the exacting principles of TS. Each nomogram shows what the stages of crushing and mass reduction will contribute to the overall precision of the FSE. Any step of the process in which the nomogram breaches the Safety Line (10% precision) or the Design Line (32% precision), should be changed to ensure that the nomogram remains consistently below these lines. In most cases the nomograms for the elements %Mn_3O_4, %FeO, %K_2O, %P, and %SO_2 are well behaved for the coarser grained materials, namely those larger than 0.9 cm. By this it is meant that the overall trajectory of the nomogram for coarser grained materials is downwards to the left, whereas the trajectory for the nomograms of finer grained materials, below 0.9 cm, is upwards and to the left, meaning they are likely to require more careful attention when designing the sampling protocol. The nomogram for K2O in fine grained Mamatwan ores is meaningless because the Alpha value derived from the calibration curve shown in Figure 9c is negative at -1.4073. Thus, the nomogram cannot be created for these ores.

Discussion and conclusions

In all the calibration curves, which should have plotted as straight lines, each element was found to have a distinctly flatter curve, in some cases even negative slopes, for materials in the finer size fractions, than for the coarser size fractions. The exact reasons for this behaviour are uncertain, but a number of reasons is suggested. The first and easiest suggestion is that it may be due to a preparation protocol in the laboratory that differed for the coarse and finer grained materials before the samples were analysed. However, one of the authors visited the laboratory to inspect the preparation protocol and has ensured that this was not the case. A second suggestion is that the distinct inflection in the calibration curves may be related to the behaviour of the crystal structure in the very pure ores as the ores are progressively milled to finer size fractions. It is possible that the component minerals, braunite, bixbyite, and psilomelane, all have different size characteristics with the dominant crystal size in the ores being about 0.9 cm. Above 0.9 cm the ores will be dominantly one ore type or another, but when the materials are crushed below 0.9 cm that the crystal structure is such that the different minerals are mixed and the behaviour of the variance for the 32 analyses is different to that for materials coarser than 0.9 cm. In all the elements analysed the Wessels ores have higher K coefficients than the Mamatwan ores; the alpha values for ores from the two mining operations are not dissimilar.

Net conclusions indicate that both Wessels and Mamatwan ores are relatively easy to sample and that simple two or three stage processing will suffice when preparing the final 2 g aliquot at 75 microns. Apart from minor modifications in the sample preparation protocols, there is no evidence to suggest that the Wessels and Mamatwan ores require different sample preparation protocols, or that they should be assayed differently. The calibration curves for manganese ore are compared with the calibration curves for gold bearing ores which generally have alpha values close to 1. The difference in alpha between the gold ores and bulk commodities is considered to be related to the primary distribution of the metals in nature, lognormal for gold and normal for manganese.

References

1. P. M. Gy, “The sampling of broken ores – a general theory”, in *Sampling Practices in the Mineral Industries Symposium*, Australian Institute of Mining and Metallurgy, Melbourne, September 16, 1976. 17p.
2. P. M. Gy, “*Sampling of particulate materials*”, Elsevier, Amsterdam. (1979).
3. P.M. Gy, “*Sampling of Particulate Materials, Theory and Practice*”, Elsevier. Amsterdam. 431. (1982).

4. P.M. Gy, Sampling of Heterogeneous and Dynamic Material Systems: Theories of Heterogeneity, Sampling, and Homogenizing, Elsevier Science Publishers B.V., Amsterdam, The Netherlands, (1992).
5. F.F. Pitard, "*Pierre Gy's sampling theory and sampling practice: heterogeneity, sampling correctness, and statistical process control*". CRC press, (1993)
6. F.F. Pitard, Theory of Sampling and Sampling Practice, third ed., CRC Press, Boca Raton, p. 691p. (2019)
7. K.H. Esbensen, "*Introduction to the Theory and Practice of Sampling*", IM Publications, Chichester, 2018, p. 327, https://doi.org/10.1255/978-1-906715-29-8. ISBN: 978-1-906715-29-8.
8. P. Thy, K.H. Esbensen and B.M. Jenkins, "On representative sampling and reliable chemical characterization in thermal biomass conversion studies", *Biomass Bioenerg.* **33,** 1513–1519 (2009). https://doi.org/10.1016/j.biombioe.2009.07.015
9. J.S. Dube, J.P. Boudreault, R. Bost, M. Sona, F. Duhaime, and Y. Ethier, "Representativeness of laboratory sampling procedures for the analysis of trace metals in soil", Environ. Sci. Pollut. Control Ser. 22 (15) 11862-11876, (2015) https://doi.org/10.1007/s11356-015-4447-1.
10. P.O. Minkkinen, K.H. Esbensen, "Sampling of particulate materials with significant spatial heterogeneity -theoretical modification of grouping and segregation factors involved with correct sampling errors: fundamental Sampling Error and Grouping and Segregation Error", Anal. Chim. Acta 1049, 47-64. (2019).
11. C.H. Tai, S.S. Hsiau and C.A. Kruelle, "Density segregation in a vertically vibrated granular bed", Powder Technology, 204 255–262. (2010)
12. R.C.A. Minnitt, P.M. Rice, C. Spangenberg, "Part 1: understanding the components of the fundamental sampling error: a key to good sampling practice", J. S. Afr. Inst. Min. Metall. 107, 505-511. (2007a)
13. R.C.A. Minnitt, P.M. Rice, C. Spangenberg, "Part 2: experimental calibration of sampling parameters K and alpha for Gy's formula by the sampling tree method", J. S. Afr. Inst. Min. Metall. 107 513-518. (2007b)
14. R.C.A. Minnitt, D. François-Bongarçon and F.F. Pitard, "Segregation Free Analysis for calibrating the constants K and a for use in Gy's formula", in: WCSB 5 Sampling. Santiago, Chile, 133-150. (2011)
15. R. Minnitt, "Calibrating K and alpha in Gy's formula: a new approach", Math. Geosci. 48, 211-232. (2016)
16. D. Francois-Bongarcon, "Geostatistical determination of Sample Variances in the Sampling of Broken Gold Ores" CIM Bulletin. 84(950), 46-57. (1991).
17. D. Francois-Bongarcon, "Geostatistical tools for the determination of Fundamental Sampling Variances and minimum sample masses". Kluwer Academic Pub. Dordrecht, The Netherlands. (1992).
18. D. Francois-Bongarcon, "The Practice of the Sampling of Broken Gold Ores" CIM Bulletin. 86(970), 75-81. (1993).
19. D. François-Bongarçon, "Introduction and first ever rigorous derivation of the liberation factor", in: Proc. 7th World Conference of Sampling and Blending (WCSB7), IM Publications, (165-168, 2015) https://doi.org/10.1255/tosf.79
20. M. Sona, J.-S. Dub_e, Sampling particulate matter for analysis – Controlling uncertainty and bias using the theory of sampling, Anal. Chim. Acta 1185 (2021), https://doi.org/10.1016/j.aca.2021.338982.
21. J.-S. Dube, M. Sona, J.-P. Boudreault, E. Hardy, Influence of particle size and grinding on measurement of trace metal concentration in urban anthropogenic soils, J. Environ. Eng. 140 (6) (2014), https://doi.org/10.1061/(ASCE)EE.1943-7870.0000825.

Appendix 1: $\%Mn_3O_4$ in 32 samples across the sample series at 15 different fragment sizes; other elements analysed include %FeO, %Al2O3, %CaO, $\%K_2O$, %P, and $\%SO_2$ which are not reported here.

$\%Mn_3O_4$	W1	W2	W3	W4	W5	W6	W7	W8	W9	W10	W11	W12	W13	W14	W15
Frag size (cm)	4.00	3.48	2.86	2.24	1.76	1.47	1.23	1.04	0.83	0.58	0.40	0.28	0.17	0.08	0.05
W1/1	37.05	68.41	76.28	61.05	61.22	65.27	63.05	65.30	64.05	64.36	65.28	64.67	64.13	64.04	62.79
W1/2	74.72	65.38	66.03	61.57	64.69	63.94	63.53	62.96	63.98	64.17	64.52	64.26	64.59	64.25	62.44
W1/3	72.78	67.04	71.58	62.43	62.97	64.26	62.76	63.43	63.14	64.19	64.95	65.00	64.30	64.14	62.46
W1/4	76.14	70.65	72.22	63.57	66.37	63.70	64.50	64.36	64.17	64.95	64.54	64.95	65.03	64.10	62.79
W1/5	59.52	74.30	66.05	61.65	63.22	65.96	66.60	64.44	65.70	65.21	64.38	64.81	64.31	64.66	62.45
W1/6	68.92	57.18	63.49	70.32	63.83	63.54	65.97	65.07	65.46	64.67	64.05	63.99	64.03	64.24	62.34
W1/7	58.21	69.35	68.88	67.15	64.36	62.71	62.95	61.42	65.44	63.31	64.09	64.83	64.27	63.85	62.75
W1/8	63.03	62.22	71.01	61.60	63.56	63.17	66.85	67.38	63.23	63.74	63.82	64.05	64.25	63.83	62.92
W1/9	58.72	65.97	64.11	64.94	67.47	65.10	63.86	65.76	64.90	65.46	64.20	64.73	64.18	63.44	62.70
W1/10	69.16	60.31	56.89	63.21	64.90	64.99	64.79	65.25	65.33	64.74	64.67	64.55	64.09	63.72	62.72
W1/11	63.35	73.71	65.70	65.18	65.97	66.18	65.68	66.75	66.85	64.74	64.49	64.37	64.66	64.08	62.55
W1/12	63.05	45.43	60.52	60.61	62.89	64.58	65.54	64.55	64.63	65.10	64.75	64.46	64.22	64.21	62.59
W1/13	67.11	67.27	69.83	70.30	67.53	63.72	66.13	63.80	64.61	65.29	64.38	64.85	63.64	64.11	62.30
W1/14	64.14	63.13	68.45	62.54	69.01	70.23	63.46	62.42	63.85	64.77	64.23	64.65	63.95	63.82	62.41
W1/15	72.47	61.37	71.08	62.21	65.75	67.43	64.55	62.93	63.94	64.61	63.50	64.49	64.09	63.84	62.22
W1/16	63.14	64.54	70.67	64.08	65.55	65.38	67.69	64.65	64.82	63.67	64.66	65.30	63.96	63.88	62.28
W1/17	73.98	69.98	61.75	63.34	66.16	63.90	64.25	64.96	63.32	64.25	64.65	64.58	64.54	63.95	62.36
W1/18	71.84	65.33	71.04	65.79	63.16	63.98	64.33	65.34	64.93	64.34	64.46	64.85	64.02	64.05	62.54
W1/19	67.68	69.92	70.35	65.26	61.36	65.41	63.82	64.32	62.74	64.37	64.54	64.27	64.23	63.95	62.41
W1/20	68.19	72.20	66.21	69.28	64.13	64.09	64.60	66.19	64.61	64.22	64.48	64.85	64.16	63.92	62.42
W1/21	51.12	73.05	67.32	65.88	62.46	67.20	64.86	64.10	64.26	64.65	65.37	64.42	64.51	63.66	62.97
W1/22	70.92	71.58	67.24	69.06	63.28	64.68	64.65	62.76	64.06	63.63	64.20	64.30	64.58	64.13	62.37
W1/23	63.71	60.64	66.62	65.40	62.20	64.67	66.05	65.40	65.10	64.65	64.50	64.90	64.25	63.94	62.52
W1/24	54.12	59.97	60.22	61.19	64.62	63.54	64.28	62.63	64.25	64.40	64.85	65.25	64.55	63.74	62.76
W1/25	72.39	66.75	71.92	70.57	61.13	61.35	64.00	63.69	62.31	64.21	65.11	64.87	64.23	64.25	62.30
W1/26	69.30	64.60	62.44	65.70	63.55	63.96	64.68	64.35	65.84	64.09	64.07	64.83	64.36	64.16	62.50
W1/27	71.56	64.47	64.53	67.39	64.43	65.73	66.43	62.88	65.84	64.65	64.91	64.90	64.26	64.09	62.07
W1/28	50.53	71.44	64.73	58.02	60.32	67.27	65.03	64.43	62.34	64.63	65.54	65.04	64.35	63.85	62.48
W1/29	71.18	69.16	67.51	63.15	64.10	66.80	63.71	64.99	64.22	64.56	64.90	64.55	63.92	63.80	62.65
W1/30	72.30	60.16	64.39	65.85	59.81	65.26	66.00	64.56	65.42	63.57	64.15	64.14	64.61	63.89	62.33
W1/31	68.98	66.95	68.41	63.95	66.09	67.03	63.28	64.96	62.12	64.90	64.06	64.30	65.06	63.84	62.42
W1/32	66.10	54.03	67.53	64.59	64.10	68.44	65.17	65.26	63.62	63.85	65.52	64.91	64.72	64.48	62.27
Average Mass	585.25	566.5	554.5	532.5	545.5	471.25	421	378.25	371.25	393.5	294.25	307.75	156.75	116	163.5